Modifications to GPS Reference Station Antennas to Reduce Multipath

Aaron Kerkhoff, R. Benjamin Harris, Colin P. Petersen, Alex Pickard
Applied Research Laboratories, The University of Texas at Austin

BIOGRAPHY

Aaron Kerkhoff is a Research Associate at the Applied Research Laboratories, The University of Texas at Austin (ARL:UT.) He received B.S degrees in both Electrical and Computer Engineering from the University of Missouri at Columbia in 1998 and M.S. and Ph.D. degrees in Electrical Engineering from the University of Texas at Austin in 2001 and 2008, respectively.

R. Benjamin Harris is an Engineering Scientist at ARL:UT. He received a B.S. (1994) and Ph.D. (2008) in Aerospace Engineering from UT Austin and his M.S. in Aeronautics and Astronautics from Stanford (2000).

Colin P. Petersen is an Engineering Scientist Associate at ARL:UT. He received a B.S. (2004) and M.S. (2006) in Electrical and Computer Engineering from UT Austin.

Alex Pickard is an undergraduate student studying Mechanical Engineering at the University of Texas at Austin.

ABSTRACT

The National Geospatial Intelligence Agency's (NGA) GPS Monitor Station Network (MSN), consisting of 11 ground reference stations distributed throughout the world, is used collaboratively by NGA and the Air Force Operational Control Segment (OCS) to monitor the health of the GPS constellation, and to generate both broadcast and precise ephemeris products. Multipath caused by signal scattering off objects in the vicinity of the antennas at these stations continues to be a dominant error source in MSN measurement observables. Both hardware-based and processing-based techniques are implemented in the MSN to mitigate this effect, however further suppression of multipath is sought in order to improve system performance.

This paper considers two different approaches to modifying the basic choke ring antenna design used in the MSN in order to reduce its reception of multipath. One approach consists of placing a large metallic ground plane directly beneath the antenna. This has the effect of shaping the antenna radiation patterns near and below the horizon so as to reduce reception of multipath signals from those directions. Another approach is to place a specific arrangement of RF absorbing foam around and beneath the base of the antenna in order to attenuate incoming multipath signals before they reach the antenna. Live-sky GPS receiver measurements were performed with a ground plane and then a novel arrangement of RF absorbing foam applied to a choke ring antenna. The results of a comprehensive analysis are presented to demonstrate the degree to which each of these approaches reduce multipath error in raw code and carrier phase observables as well as in carrier phase smoothed observables used in the GPS precise ephemeris production process.

INTRODUCTION

The Applied Research Laboratories at the University of Texas at Austin (ARL:UT) maintains, in partnership with the National Geospatial Intelligence Agency (NGA), a worldwide network of 11 unmanned Global Positioning System (GPS) reference stations, known as the Monitor Station Network (MSN). NGA collects, processes, and distributes GPS observations, environmental data, and station health information from the MSN on a 24/7/365 basis. MSN data is used for a number of purposes by both NGA and the Air Force Operational Control Segment (OCS), including monitoring the quality and quantity of GPS satellite observables, and the generation of broadcast and precise ephemeris products [1].

Multipath error caused by signal scattering off objects near the antenna was an important consideration in the design of the MSN and multiple techniques were implemented to reduce its effect. At each MSN site, the antennas are elevated above nearby structures as much as is possible in order to minimize multipath components emanating from above the horizon. Choke ring antennas are used, which significantly attenuate multipath impinging from near the horizon and below the antenna. Processing

23rd International Technical Meeting of the Satellite Division of
The Institute of Navigation, Portland, OR, September 21-24, 2010

methods are implemented in the receiver tracking loops, which further reduce multipath error in the measured observables. Finally, post-processing techniques are used to reduce the impact of multipath in data products, such as precise ephemerides, derived from the raw measurements.

Despite these efforts, multipath continues to be a dominant error source in MSN measurement observables. An analysis was performed on multiple years of MSN data to determine typical levels of multipath at each station. Fig. 1 provides a visualization of the mean multipath error on the ionospheric-free (L3) code multipath observable as a function of elevation and azimuth angles relative to the antenna at the England MSN site. The method for creating this plot is described later in this paper. A number of concentric rings of alternating color (intensity) are evident in the plot, which are the wave interference pattern caused by the interaction of the direct satellite signal and multipath scattering off the ground and other objects near the antenna. Note that in some directions, the mean level of multipath in this observable exceeds 1 m. Similar results were found in all of the other MSN stations.

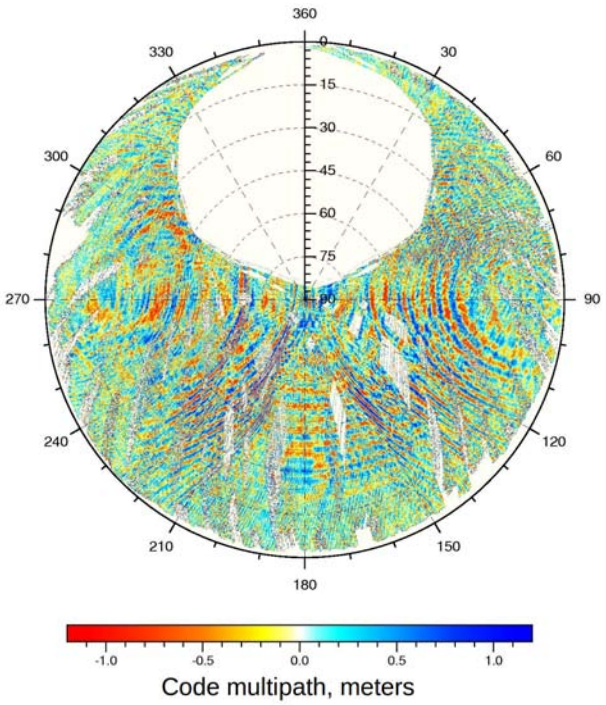

Fig. 1 Mean multipath error on L3 code multipath observable as a function of elevation (radial component) and azimuth (angular component) angles relative to England MSN antenna. Note that the hole at the top of the plot is due to the lack of satellite observability at those directions.

A common post-processing approach to mitigate multipath is carrier phase smoothing of the code observable. This practice dates back as far as the Hatch filter [2], and is commonly used within GNSS receivers. NGA employs carrier phase smoothing to condition all of the raw observable used in generating GPS precise ephemerides. However, as demonstrated analytically in [3], multipath error in the raw observables does indeed translate to a bias in the smoothed observables. This is due to the fact that the smoothing process acts like a low pass filter, and thus, low frequency error components cannot be removed.

Multipath error is a concern for other GNSS ground reference station besides the MSN. In [4], an analysis of two years of data from over 200 International GNSS Service (IGS) and U.S. Continuously Operating Reference Station (CORS) network sites demonstrates that each site exhibits a repeating pattern in post-fit carrier phase residuals due to multipath and that the amplitude of this effect is strongly influenced by the type of antenna used. A multi-year analysis of data from many IGS stations [5] suggests that near-field multipath effects between the antenna and its surroundings may lead to annual variations in estimated site positions at the 1 to 2 cm level. As indicated in [6], if not mitigated, multipath error would consume 90% of the error budget for the Local Area Augmentation System (LAAS) used to assist civil aircraft landing. As such, a sophisticated antenna design has been developed for LAAS to reduce multipath to an acceptable degree.

In the present study, we consider modifying the existing choke ring antennas used at MSN stations so as to reduce their reception of multipath, particularly those components emanating from near and below the horizon. One approach is to place a large metallic ground plane directly underneath the choke ring antenna. The ground plane interacts with the antenna in such a way as to modify the shape of the antenna radiation patterns. With the appropriate sizing of the ground plane, it is possible to tailor the shape of patterns to reduce signal reception at lower angles, and thus reduce multipath. Such an approach was implemented at the U.S. Air Force GPS Monitor Stations as part of the Monitor Station Antenna Replacement (MSAR) project [7]. Another approach is to place lossy material near the antenna in order to attenuate impinging multipath signals before they reach the antenna. A novel arrangement of outdoor-rated RF absorbing foam placed around and underneath the antenna for this purpose is described in this paper.

A measurement campaign was conducted to evaluate the efficacy of augmenting a choke ring antenna with a metallic ground plane or RF absorbing foam to mitigate multipath. Long-term GPS data collections were performed with each of these configurations using an equipment setup identical to an MSN station. An analysis was performed on raw code and carrier phase receiver observables, as well as carrier phase smoothed observables used in NGA's precise ephemeris production process to determine the degree to which each configuration reduces multipath.

This paper is organized as follows: First, the ground plane and RF absorbing foam approaches to multipath mitigation are described in greater detail. Then the test setup

used in measurements and the data analysis approach are described. Next, the results of data analysis are given. Finally, conclusions are made.

ANTENNA MODIFICATIONS

Since antennas at MSN sites are typically raised above all nearby objects and structures, it is assumed in this case that multipath error is caused primarily by signals scattered off of objects below the antenna. In many cases, the dominant multipath component is caused by specular reflection off a large, relatively flat surface such as the ground or the roof of the building on which the antenna is mounted. Multipath may also be caused by signal diffraction off of objects in the vicinity of the antenna such as building edges, railings, or antenna stands.

It is necessary to consider the polarization of GPS signals to determine the desired characteristics of the antenna. The polarization of a direct GPS signal is right hand circular (RHCP.) A GPS signal specularly-reflected off a horizontal surface such as the ground exhibits left hand circular polarization (LHCP) due to a 180 degree phase shift induced by reflection; the exceptions to this are relatively low elevation angle reflections, occurring below Brewster's angle, which exhibit RHCP due to an additional 180 degree phase shift [8]. Diffracted signals are typically elliptically polarized, exhibiting both RHCP and LHCP components.

One way to reduce multipath reception is to shape the antenna radiation patterns to achieve high RHCP gain towards elevation angles above the horizon to receive the direct component and low gain towards angles below the horizon to reject multipath. Another approach is to take advantage of the change in signal polarization due to scattering by designing the antenna to have very low LHCP gain at all elevation angles both above and below the horizon.

The commercial electromagnetic software HFSS [9] was used to simulate the response of a typical choke ring antenna. The choke ring antenna radiation patterns, which are shown in Fig. 2 for the L1 frequency, exhibit relatively low LHCP gain over all elevation angles, high RHCP gain above the horizon, and typically low RHCP gain below. However, just below the horizon, the slow rate of roll-off in the RHCP pattern leads to higher than desired gain in those directions. To further reduce multipath reception as compared with a typical choke ring antenna, it is desired to increase the rate of RHCP pattern roll-off near the horizon and if possible, decrease LHCP reception, particularly below the horizon.

Ground Plane

A straightforward way to modify the radiation patterns of a choke ring antenna is to place a large metallic ground plane directly beneath it, as depicted in Fig. 3. This approach was first considered for the U.S. Air Force

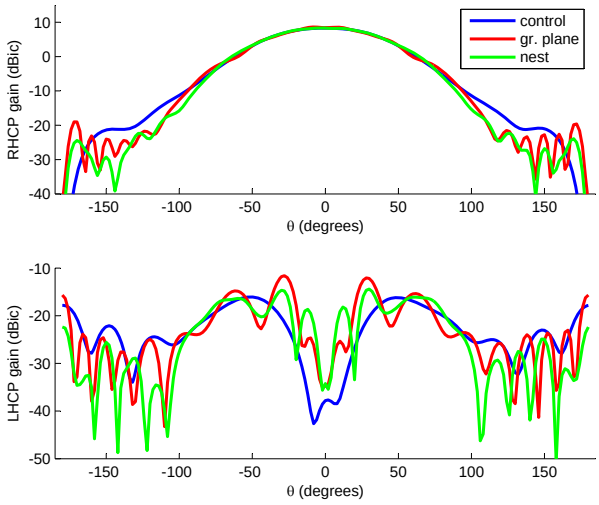

Fig. 2 Comparison of simulated radiation patterns for choke ring only (control), choke ring with a 1.22 m circular ground plane, and choke ring with the RF absorbing foam nest at L1 frequency. Note that the patterns are plotted in terms of zenith angle, θ.

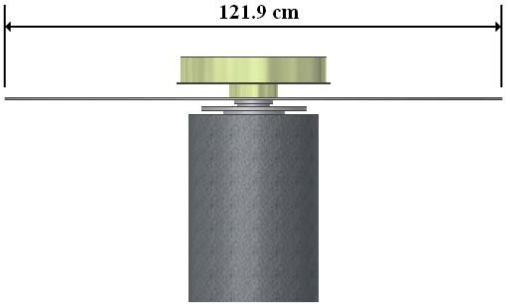

Fig. 3 Arrangement of the ground plane beneath the choke ring antenna.

MSAR [7] project where it was found that installing a 0.91 m (3 foot) diameter circular ground plane directly beneath the choke ring improved raw GPS observable statistics due to a reduction in multipath. In an preliminary study, where we considered ground planes of varying sizes and shape, we found that good results could also be achieved by mounting a larger, 1.22 m (4 foot) diameter circular ground plane at a slightly lower location relative to the bottom of the choke ring, as shown in Fig. 3. This ground plane location was chosen to simplify its mounting on the antenna stand.

Fig. 2 includes the simulated L1 radiation patterns that result from adding the 1.22 m ground plane to the choke ring antenna. As compared with the original choke ring antenna, the addition of the ground plane causes a reduction in the RHCP gain beginning at the horizon ($|\theta| = 90\,^\circ$,

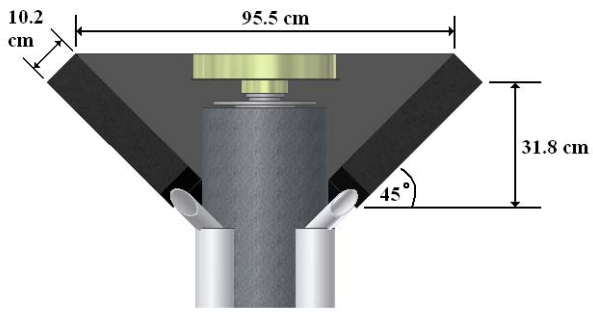

Fig. 4 Cut-away view of the RF absorbing foam nest.

where θ is the zenith angle) and continuing for most angles below. It is noted though, that the ground plane enhances the RHCP gain at some very low angles, near $|\theta| = 160^\circ$ This is deemed a reasonable trade-off since the gain at high elevation angles above the horizon is still much higher ($\geq$ 28 dB) than at corresponding angles below the horizon. A similar trade-off must be made in the LHCP performance by adding the ground plane. For most angles below the horizon, the LHCP gain is reduced as compared with the original choke ring, as desired, while for most angles above the horizon the LHCP is increased. Again, this trade-off is tolerable since most scatterers are intentionally kept below the horizon of the antennas at MSN sites. Similar trends are evident in the radiation patterns at the L2 frequency.

RF Absorbing Foam

Another approach to reduce multipath is to place lossy material near the antenna so as to attenuate scattered signals before they reach the antenna. Radio frequency (RF) absorbing foam is an attractive option for this application since it is commercially available from a number of manufacturers and is reasonably low cost. Fig. 4 illustrates an arrangement of shaped RF absorbing foam blocks placed around and relatively near a choke ring antenna so as to reduce multipath from elevation angles near the horizon and below. The foam extends from the top edge of choke ring surface to well below the bottom edge of the antenna in order to completely shield it from incident signals from below. A sufficient opening is left between the bottom edges of the foam pieces so that the entire assembly can fit over the antenna stand for convenient mounting. This structure will be referred to as the RF absorbing foam 'nest' in the remainder of this document.

Cuming Microwave C-RAM AR, an open-cell foam impregnated with a lossy material and rated for outdoor use, is used in this application. The loss is graded along the thickness of the C-RAM foam in order to provide both high transmission loss (attenuation of the incident wave) and low reflectance from the front surface of the foam. A foam thickness of 10 cm (4 inches) was selected in order to provide high attenuation in the 1 to 2 GHz frequency band. The foam is designed to exhibit good performance over an incident angular range of +/- 45 $^\circ$ from normal.

The overall height and width of the nest were selected to provide a reasonable trade-off between cost and performance. In principle, a larger RF absorbing foam structure could exhibit improved performance by providing a larger stand-off distance so that it interacts less with the antenna. On the other hand, increased material costs and installation complexity are associated with a larger structure. The foam tilt angle of 45 $^\circ$ was selected so that the foam would exhibit reasonable attenuation regardless of the angle at which a wave impinges upon it from below. The higher loss side of C-RAM foam was intentionally pointed away from the antenna in order to minimize reflections from the inside surface of the foam.

The combination of the choke ring antenna and RF absorbing foam nest was simulated and the resulting L1 radiation patterns are included in Fig. 2. As compared with the ground plane, the nest provides only a slight improvement in RHCP pattern roll-off near the horizon, but significant reduction in RHCP gain for $|\theta| \geq 130^\circ$. Additionally, the LHCP gain with the nest is reduced as compared with the ground plane over most angles above and below the horizon, though somewhat enhanced as compared with the original choke ring near the zenith. Similar trends are evident at the L2 frequency.

These results suggest that some reduction in multipath reception should be provided by adding the ground plane beneath the choke ring antenna, but that further reduction should be provided by using the RF absorbing foam nest instead.

MEASUREMENT APPROACH

Each antenna under test (AUT) was placed on a 1.52 m (5 feet) tall antenna stand on the roof of the ARL:UT main building. New GPS equipment, currently being deployed to each of the MSN stations, was used for this measurement campaign. This includes a geodetic-quality ITT Corporation Selective Availability / Anti-Spoofing (SAASM) Module GPS receiver, as well as an antenna consisting of an ITT choke ring and a Dorne-Margolin element. The new ITT receivers output all code / carrier combinations for up to 12 satellites on L1 C/A, L1 P/Y, L2 P/Y, and L2C with better data availability and precision than the outgoing Ashtech Z(Y)-12 receivers. As compared with the old Ashtech choke ring antennas, the ITT choke ring antennas provide a higher pre-amp gain and contain an integrated temperature sensor. As is typical of MSN operations, the ITT receiver was syntonized to a Symmetricom 5071a cesium frequency standard throughout testing. Note that this equipment setup is identical to that implemented at MSN stations, and thus the results presented here should be representative of an MSN station.

Fig. 5 Configuration of the choke ring-only (control) test case at the AUT site (right) and choke ring mounted at the REF site (left.) The REF site is only used for carrier phase analysis.

To support differential analysis of carrier phase multipath, as will be discussed later in this paper, another ITT choke ring antenna was placed on a highly stable survey monument in a flat, open field located roughly 200 m from the AUT site. The antenna is connected by buried coaxial cable to an air-conditioned hut housing an ITT receiver. This receiver is syntonized to a rubidium frequency standard as no additional cesium standards were available for this effort. This site will be referred to as the REF site in the remainder of this paper.

Fig. 5 shows the AUT site configured for the choke ring-only (control) test and the configuration of the REF site for all tests. Fig. 6 shows the configuration of the ground plane beneath the AUT choke ring antenna. The ground plane was constructed of 3.2 mm thick aluminum to withstand moderate wind loading and was mounted parallel to the surface of the roof. Fig. 7 shows the installation of the RF absorbing foam nest around the AUT choke ring. A temporary PVC structure was constructed to support the pieces of Cuming Microwave C-RAM, which were cut out of 10 cm thick, 0.61 m (2 foot) by 0.61 m blocks. Velcro straps were used to hold the foam in place.

Roughly week-long data collections were performed for each AUT case. The dates of data collection were day of year (DOY) 135-142, 2010 for the control case, DOY 159-165, 2010 for the ground plane case, and DOY 170-176, 2010 for RF absorbing foam nest case. In each case, dual frequency P(Y) observables were logged at both the AUT and REF sites at a 1.5 second rate.

ANALYSIS APPROACH

The effects of adding the ground plane or the RF absorbing foam nest to the choke ring antenna are evaluated through the analysis of raw code observables, raw carrier phase observables, as well as the smoothed observables

Fig. 6 Configuration of the ground plane test case at the AUT site.

Fig. 7 Configuration of RF absorbing foam nest test case at the AUT site.

used in generating precise ephemeris products. The approach used in analyzing each type of observable is described below.

Code Multipath Observables

Kee and Parkinson defined the Dual-Frequency Method (DFM) as a way to create an empirical map of code multipath on L1 at a static reference site [10]. In this study, we use a modified version of the DFM. For each AUT case, three empirical models were formed, which are dominated by multipath on the L1, L2, and L3 P(Y) code observables, respectively; L3 refers to the ionospheric-free combination of observables.

The input to the DFM are observations that can be formed into an ionosphere-free linear combination. These observations are then differenced to remove common mode errors such as troposphere delay, clock and relativistic errors. These final differences are dominated by bias, multipath and noise processes.

Kee and Parkinson defined a linear combination, which

uses dual frequency code and carrier phase observables. These observable are defined as follows:

$$\begin{aligned}
\rho_{P1} &= d + c\delta t + i_{L1} + \nu + t + M_{P1} + \epsilon_{P1} && (1)\\
\phi_{P1} &= d + (N_{P1} + \varphi_{L1})\lambda_{L1} + c\delta t - i_{L1} + \nu \\
&\quad + t + m_{P1} + \eta_{P1} && (2)\\
\rho_{P2} &= d + c\delta t + \gamma i_{L1} + \nu + t + M_{P2} + \epsilon_{P2} && (3)\\
\phi_{P2} &= d + (N_{P2} + \varphi_{L2})\lambda_{L2} + c\delta t - \gamma i_{L1} + \nu \\
&\quad + t + m_{P2} + \eta_{P2} && (4)
\end{aligned}$$

where the symbols are defined as:

ρ pseudorange (or code) observable

ϕ carrier phase observable

d true distance traveled by the signal

c the speed of light

δt difference in clock offsets between the satellite and receiver

i ionosphere delay

γ ratio of delays between L1 and L2: $\gamma = \left(\frac{f_{L1}}{f_{L2}}\right)^2$

ν relativistic delay

t troposphere delay

M pseudorange multipath

m carrier phase multipath

ϵ thermal noise on pseudorange

η thermal noise on carrier phase

The series of observable combinations used to isolate code multipath are well documented by Kee and Parkinson [10] and Harris [11]. Here we simply restate the final multipath combination and the solution to its error terms. The first combination which represents an estimate of the multipath on the L1 code observable, denoted μ_1, is defined as follows:

$$\mu_1 = \rho_{L1} - \phi_{L1} + \frac{2}{1-\gamma}(\phi_{L1} - \phi_{L2}) \qquad (5)$$

Substituting the observables in Eqs. 1, 2 and 4 into the combination defined in Eq. 5 results in a quantity that takes the following form:

$$\mu_1 = m + B_\mu + \epsilon \qquad (6)$$

where

$$\begin{aligned}
m &= M_{P1} - m_{P2} + \frac{2}{1-\gamma}(m_{P2} - m_{P1})\\
B_\mu &= \left(\frac{1+\gamma}{1-\gamma}\right)(N_{P1} + \varphi_{L1})\lambda_{L1}\\
&\quad - \left(\frac{2}{1-\gamma}\right)(N_{P1} + \varphi_{L2})\lambda_{L2}\\
\epsilon &= \epsilon_{P1} - \eta_{P1} + \frac{2}{1-\gamma}(\eta_{P1} + \eta_{P2})
\end{aligned}$$

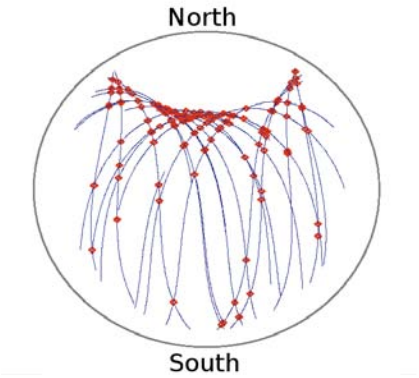

Fig. 8 Overhead passes as observed from a static reference site in the northern hemisphere. The intersections between each pass are marked.

The term m is dominated by the multipath associated with the code observable. The bias term B_μ is constant for each overhead pass, as long as the carrier phase is tracked without discontinuity (e.g., a cycle slip). Contributors to the bias term include not only carrier phase ambiguity but also delays contributed by receiver and satellite hardware biases. Combinations corresponding to the multipath on L2 and L3 code observables are:

$$\begin{aligned}
\mu_2 &= \rho_{L2} - \phi_{L2} + \frac{2\gamma}{1-\gamma}(\phi_{L1} - \phi_{L2})\\
\mu_3 &= \rho_{L1} - \phi_{L1} + 1.54573\,(\rho_1 - \rho_2 - \phi_{L1} + \phi_{L2})
\end{aligned}$$

The DFM process provides a means to estimate the bias differences between each pair of overhead passes. That process relies on overhead passes having intersections as seen from the receiver-centered or topocentric frame. In Figure 8, one day of passes and their intersections are depicted. At each intersection, code multipath observables, μ_k, where k is frequency, are differenced between passes. If the number of intersections exceeds the number of passes, this forms a set of overdetermined equations that describe the bias difference between passes. Once those bias differences are removed from each pass, the resulting modified μ_k are biased by a single, common bias. This final bias can be solved by relying on a zero mean condition present in code multipath. This condition is met by multipath induced by ground reflections as they approach the horizon [3]. In sites where the dominant reflector is the ground, this fact can be used as a constraint to solve for the final bias.

Single Difference Carrier Phase Observables

The approach used to analyze raw carrier phase observables is essentially identical to one described in [12] for GPS antenna phase center variation (PCV) calibration. This approach makes use of single differences (SD) of carrier phase measurements of a common satellite from two

antennas separated by a short distance, which provides cancellation of many error terms including those due to satellite orbits and clocks and the atmosphere. In this way it is possible to resolve antenna-related characteristics such as PCVs, or in the case of the present study, multipath reception with mm-level precision. As described in the previous section, a reference antenna (REF) used in this analysis is placed in a relatively flat, open field, which is a relatively short distance (roughly 200 m) from the AUT site.

The observation equation for the single difference carrier phase measurement between stationary sites A and B, to satellite i at time τ is

$$\Delta\Phi^i_{A,B}(\tau) = \Delta d^i_{A,B}(\tau) + N^i_{A,B} + \delta t_{A,B}(\tau) + m^i_{A,B}(el^i(\tau), az^i(\tau)) + \eta^i_{A,B}(\tau) \quad (7)$$

where $\Delta\Phi^i_{A,B}$ is the measured SD carrier phase, $\Delta d^i_{A,B}$ is the SD satellite to antenna geometric range, $N^i_{A,B}$ is the combined phase ambiguity term (constant over a satellite pass assuming no cycle slips), $\delta t_{A,B}$ is the residual clock offset between the two receivers, $m^i_{A,B}$ is the combined multipath error at the two sites and $\eta^i_{A,B}$ is the combined receiver noise term. Note the fact that the multipath error in a measurement at a given site is purely a function of satellite elevation, el, and azimuth, az, angles, has been included explicitly in this expression. The SD satellite to antenna geometric range term can be expanded using

$$\Delta d^i_{A,B}(\tau) = \overrightarrow{b}_{A,B,REF} \cdot \hat{r}^i(\tau) + \Delta\overrightarrow{h}_{A,B} \cdot \hat{r}^i(\tau) + \delta\phi^i_{A,B}(el^i(\tau), az^i(\tau)) \quad (8)$$

where $\overrightarrow{b}_{A,B,REF}$ is the baseline vector between the reference surfaces upon which the reference antenna and AUT are mounted, $\hat{r}^i$ is the line of sight vector between the antenna and satellite i (which is assumed to be identical for the two antennas in the current effort since they are closely spaced), $\Delta\overrightarrow{h}_{A,B}$ is the difference in the average phase center offset (PCO) vectors of the reference antenna and AUT, and $\delta\phi^i_{A,B}$ is the difference in the phase center variation (PCV) between the reference antenna and AUT in the direction of satellite i, where again the dependence on satellite direction has been indicated explicitly. This development assumes that the average PCO vector of each antenna is determined relative to the reference surface on which the antenna is mounted, and the PCVs of each antenna are referenced to its PCO.

The baseline vector between the two antennas, and the antenna PCOs have each been determined to sub-mm precision by means of precise double difference carrier phase methods. Combining Eqs. 7 and 8, and moving all measured or known quantities to the left side yields (note that the time dependence has been suppressed for clarity)

$$\Delta\Phi^i_{A,B} - \overrightarrow{b}_{A,B,REF} \cdot \hat{r}^i - \Delta\overrightarrow{h}_{A,B} \cdot \hat{r}^i = \delta\phi^i_{A,B}(el^i, az^i) + N^i_{A,B} + \delta t_{A,B} + m^i_{A,B}(el^i, az^i) + \eta^i_{A,B} \quad (9)$$

which provides an observation equation relating the SD carrier phase measurements to the quantity of interest, the multipath error.

SD observables as defined by Eq. 9, are calculated for each satellite pass in the data set. Next, an autonomous code-based clock solution is calculated for each site, and a low-order polynomial is fit to each. These polynomials are used to time align the measurements from the two sites and remove a bulk clock estimate from the SD observables. A weighted least squares approach is used to estimate a number of the terms on the right side of Eq. 9. A polynomial is used to estimate the combined antenna PCVs; note that only the elevation dependence of the PCVs is considered here. A combined receiver clock state is included for each measurement epoch to absorb residual clock offset between receivers, and a (floated) phase ambiguity term is included for each satellite pass. Outlier removal and cycle slip correction are performed prior to and between iterations of the least squares estimator. Measurements are weighted by $sin(el)$ in the estimator.

Once estimation is complete, all of the estimated terms are subtracted from the original SD observable to form a residual, which contains only multipath and receiver noise. As described later in the paper, statistics are calculated on this residual to assess multipath performance. This analysis is repeated for each GPS frequency.

Carrier Phase Smoothed Observables

As discussed earlier, NGA applies a carrier phase smoothing process, which we will refer to as the 'smoother', to raw observables prior to generating the precise ephemeris product. The first step in creating smoothed observables is to generate the ionosphere free (IF) combination on both raw code and carrier phase observables. Then the smoother interpolates the IF carrier phase observable so that it represents a measurement collected in regular intervals of GPS time. Finally, the bias between the IF code and carrier phase is estimated and added to the interpolated carrier phase to produce a carrier phase smoothed pseudorange. Further details associated with the smoothing process are defined as a technical report [13].

In this study, the input data rate to the smoother was set at 1.5 seconds, while the output data rate was set to 5 minutes. The smoother can be configured in one of two smoothing modes, 1) a moving window mode, in which only data between two consecutive output epochs are used to form a given smoothed observable, or 2) a continuous pass mode in which all of the data from the beginning of a pass up through most current output epoch is used to form a smoothed observable. The continuous pass mode is currently in use by NGA for precise ephemeris generation as it leads to lower noise in the observables than the moving window mode. However, continuous pass smoothing tends to smear multipath effects over a wider range of incidence angles than they actually occur. The moving win-

dow smoother, on the other hand, maintains the true spatial dependence of multipath errors, which is of particular interest in this study and simplifies the comparison of results from different AUTs. Therefore, moving window smoothing was used in this study. The evaluation of multipath effects on smoothed observables generated using continuous pass smoothing will be addressed in a future study.

The quality of the smoother products can be assessed by differencing the smoothed pseudorange from a truth source for pseudorange. This difference is referred to here as an *Observed Range Deviation (ORD)*. NGA Precise ephemerides are used as the truth source. The ORD calculations were computed using applications design specifically for this task, which are part of the GPS Toolkit (GPSTk), an open-source library and suite of applications for GNSS data processing developed and maintained by ARL:UT [14].

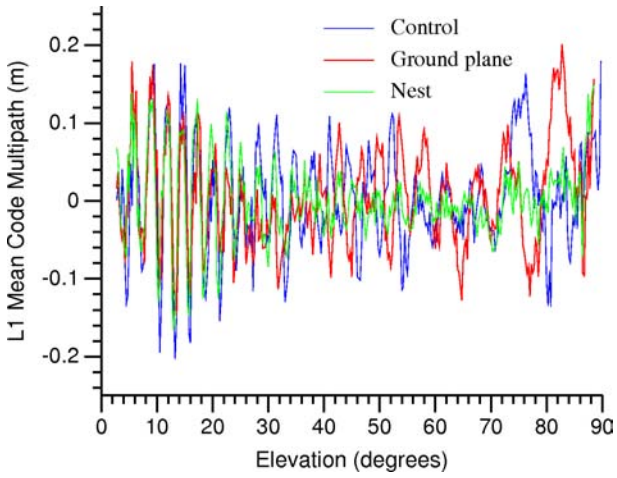

Fig. 9 Binned mean of L1 code multipath observables.

RESULTS

Code Multipath Observables

The DFM, as described in the previous section, was used to generate observables corresponding to P(Y) code multipath on the L1, L2, and L3 frequencies for each AUT case. These observables were generated at the full data collection rate of 1.5 sec. For each AUT case and frequency, the code multipath observables are sorted in terms of elevation angle, and binned statistics are calculated in 0.25 ° bins.

The binned mean and rms of L1 code multipath observables for the three AUT cases are compared in Fig. 9 and 10. The trend in mean code multipath with elevation angle is dominated by specular reflection off of the roof and ground at the AUT site, and is influenced by two factors. One factor is that the ratio of direct to reflected signal amplitudes decreases, and thus multipath amplitude increases, with decreasing elevation angle primarily due to radiation pattern roll-off in the antenna. The second is the nature of the multipath envelope of the receiver code tracking loop. This envelope goes to zero for zero delay between direct and reflected signal components, which occurs for ground-bounce multipath at el = 0 °, and increases with increasing delay, or elevation angle, before plateauing at some delay value [15]. As such, high mean code multipath may occur over a wide range of elevation angles, both low and high, which is evident in the results for the control case. The code multipath rms exhibits a different trend than the mean, one that is essentially monotonically increasing with decreasing elevation angle. Note that at lower elevation angles the rms values are much higher than the mean values, which suggests that there is a high level of noise in the code observable at these angles, possibly due to non-specular, diffuse scatter.

As compared with the control case, the use of the ground plane appears to offer little improvement in the L1 mean for el ≥35 ° with perhaps some degradation near the zenith. Above approximately el = 20 ° the L1 rms with the ground plane is generally comparable to the control case except near el = 58 ° where the ground plane rms peaks up. This peak was found to be repeatable between consecutive days, and thus is a multipath effect. This could be due to a scatterer that was illuminated in the ground plane test, but not in the other tests due to the precession of satellite orbits between the times that the tests were conducted. The enhancement of LHCP gain at this elevation angle due to adding the ground plane, which is evident in Fig. 2, could also contribute to this effect. At lower elevation angles, however, the ground plane offers significant reduction in both the L1 mean and rms as compared with the control case.

The use of the RF absorbing foam nest offers a significant reduction in the L1 mean at higher elevation angles as compared with both the control and ground plane cases, though the values are comparable to the ground plane below el = 35 °. On the other hand, the nest exhibits much lower L1 rms values over nearly all angles than the other two cases.

The binned mean and rms of L3 code multipath observables for the three AUT cases are compared in Fig. 11 and 12. The mean and rms code multipath values for all three AUT cases are significantly higher for the L3 observable than the L1 observable as expected due to the mulitpath amplifying effect of the ionospheric-free observable. Otherwise, the three AUTs perform similarly relative to one another at L3 as at L1. While the ground plane exhibits a slightly better L3 rms than the control case at some higher elevation angles, the peak at el = 58 ° persists and some degradation near the zenith is evident. The ground plane offers significant reduction in the L3 rms below approximately el = 20 ° while the RF absorbing foam nest does so over nearly all angles.

Table 1 provides the total code multipath rms statistics calculated over all observables (elevation angles) for each

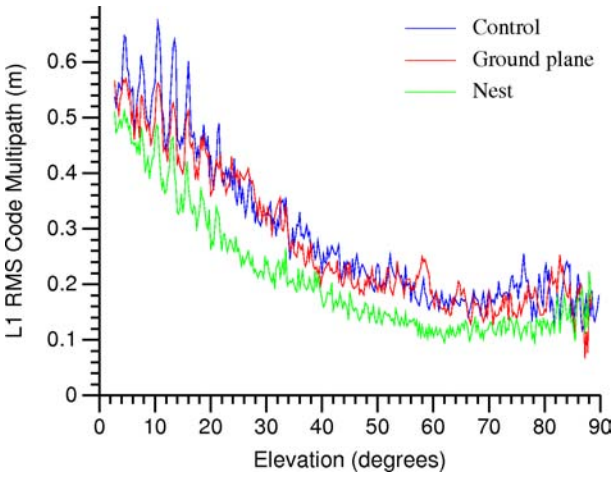

Fig. 10 Binned rms of L1 code multipath observables.

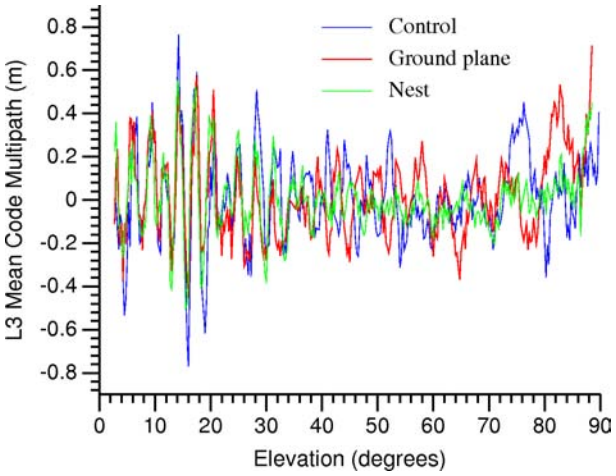

Fig. 11 Binned mean of L3 code multipath observables.

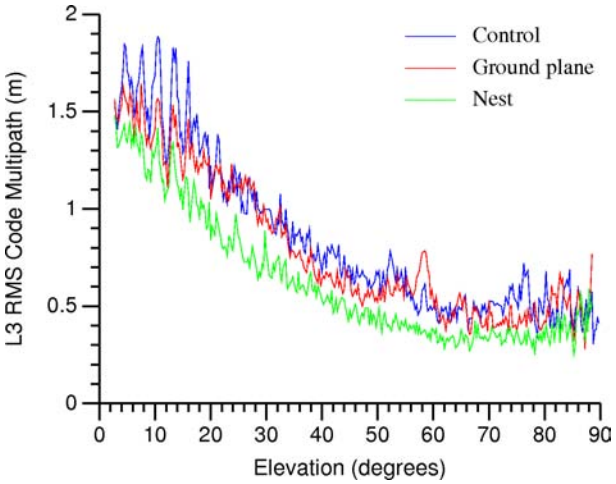

Fig. 12 Binned rms of L3 code multipath observables.

Table 1 Total code multipath rms error (in meters) for each case and frequency combination. Percentages indicate reduction relative to the control case.

	L1		L2		L3	
Case	RMS	%	RMS	%	RMS	%
Control	.379	-	.358	-	1.11	-
Gr. plane	.353	6.9	.302	15.6	1.01	9.1
Nest	.283	18.5	.288	19.4	.841	24.3

AUT case and frequencies. Both the ground plane and RF absorbing foam nest provide a reduction in the total rms as compared with the control case at all three frequencies. The ground plane performs much better at L2 than at L1 while the nest performs similar at both frequencies. At L3, however, the nest provides significantly better performance than the ground plane.

Single Difference Carrier Phase Observables

As described in a previous section, SD carrier phase post-fit residuals are generated from the data for each AUT. This processing is performed at a 30 second rate, rather than the full 1.5 second data rate, due to memory limitations in the processing scripts used. A multi-day dataset is first processed in a number of 12 hour batches. Then, the post-fit residuals from all batches are combined to form a single set of residuals for the entire dataset. The final set of residuals are sorted in terms of elevation angle, and consistent with the pseudorange analysis above, are used to calculate binned statistics with a bin size of 0.25 °.

A few comments should be made concerning the analysis of SD carrier phase observables. Unlike the pseudorange analysis above, this is a differential technique, and thus the results will exhibit effects, including multipath error, due to both the AUT and the REF antenna. This has been partially mitigated by placing the REF antenna in a flat, open field, well away from structures that may cause signal scattering. Nonetheless, the ground bounce multipath component at the REF site is non-negligible, and will contaminate the final results. Another issue complicating analysis of carrier phase observations is antenna PCV, which exhibit amplitudes comparable to carrier phase multipath. This is dealt with by using like-type antennas at the AUT and REF so that the PCV largely cancel in the SD carrier phase observables. However, the PCV may be altered by making modifications to the AUT.

These effects are demonstrated in Fig. 13, which shows the L1 SD carrier phase elevation-binned means for each of the AUT considered in this study. In this case, no PCV polynomial has been estimated and removed in residual processing. The high frequency oscillations due to multipath, are clearly altered by each of the modifications to the

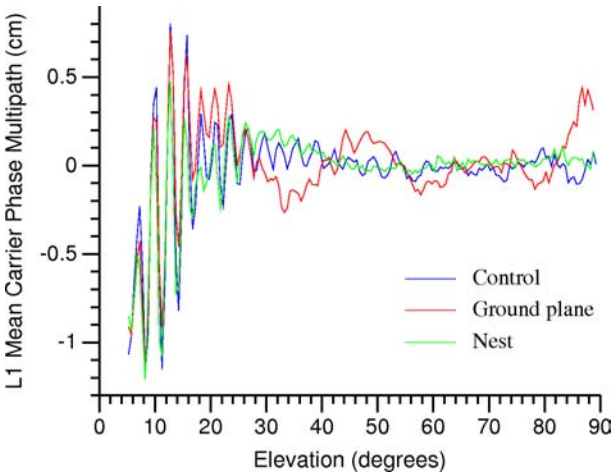

Fig. 13 L1 binned mean for raw carrier phase observable when no PCV is estimated in residual processing.

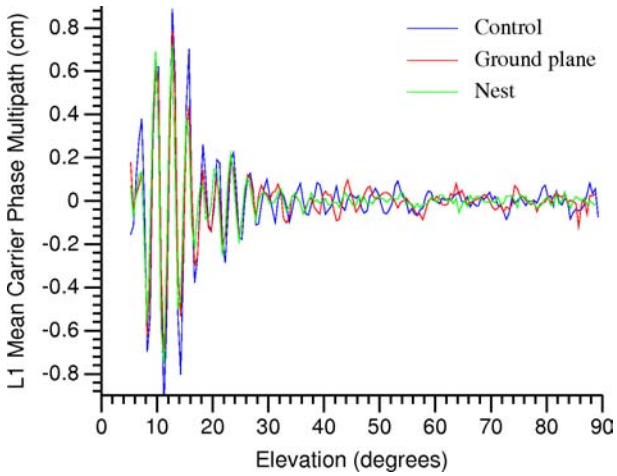

Fig. 14 L1 binned mean for raw carrier phase observable when a 10th order polynomial PCV is estimated in residual processing.

choke ring antenna. However, there is a common downward trend at low elevation angles in all three results. This trend is believed to be due to, primarily, the multipath at the REF site, which does not change between tests. Also, note that a low frequency oscillation develops when the ground plane is added to the choke ring; this was determined to be due to a change in the antenna PCV. This change in PCV between tests makes it difficult to compare the multipath behavior of different AUT. Therefore, the residual processing was re-run including a 10th order polynomial to account for antenna PCV. This was done for each AUT case for consistency. As is evident in the results given below, this not only removes any trend due to PCV, but also other low order trends in the data. This includes any bulk component of low elevation multipath at the AUT site. This, and the differential nature of the measurements likely make the estimates reported here of the reduction in carrier phase multipath provided by each antenna modification somewhat conservative.

The SD carrier phase elevation binned mean and rms statistics for the three AUTs (when a 10th order PCV polynomial is estimated in processing) are compared for the L1 and L3 frequencies in Fig. 14, 15, 16, and 17. The statistics for all three AUT exhibit a generally monotonically increasing trend with decreasing elevation. This is due primarily to the nature of the multipath envelope of the receiver carrier phase tracking loop, which typically exhibits increasing multipath error with decreasing delay [15]. Note, however, that there is some decrease in the statistics below $el = 10^\circ$. This is due to removing a PCV estimate from the residuals, which also removes a low order multipath component, as discussed previously.

Similar trends in the mean statistic between different AUT are evident in the SD carrier phase multipath observable as in the code observable. For both L1 and L3, the variation in the mean using the ground plane is comparable to the control case at higher elevation angles, but improved at lower elevation angles. The mean using the nest, on the other hand, is improved relative to the control case over nearly all angles. At lower elevations, below $el = 15^\circ$ at L1, and $el = 40^\circ$ at L3, the improvement in the mean is comparable for the ground plane and nest cases.

Some differences, however, are noted in the carrier phase statistics as compared with the code statistics. Though the ground plane exhibits improvement in the L1 SD carrier phase rms at lower elevation angles, it exhibits degradation above $el = 20^\circ$. In the code results, however, the ground plane only exhibits degradation in the L1 rms statistic near $el = 58^\circ$. This difference in the behavior of the two observables is not yet understood. Also note that while the nest L1 rms is much better than the control case at lower elevations, it appears to offer no improvement above $el = 25^\circ$; this is also contrary to the code observable results. It is believed that at higher elevation angles, a precision limit in the carrier phase residual processing is being reached so that it is not possible to resolve improvement due to the nest in single frequency results. This hypothesis is supported by the L3 rms statistics, which are somewhat better with the nest than the control case at higher elevation angles. The amplifying effect of the L3 observable causes the observable noise to raise above the precision limit in residual processing.

Summary rms statistics calculated over the entire set of residuals (all elevation angles) for each AUT case and L1, L2, and L3 frequencies are given in Table 2. Consistent with the results for the code observable, both the ground plane and the absorber nest offer an improvement in the total carrier phase residual rms at all frequencies considered, but the nest performs somewhat better in each case. In general, the improvement to the carrier phase observable offered by these antenna modifications is somewhat lower

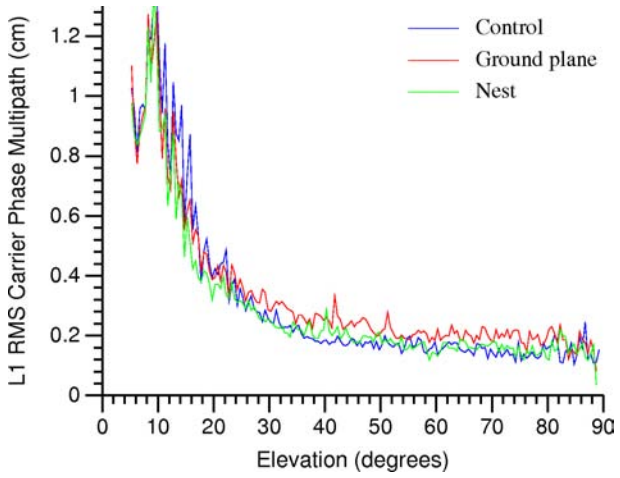

Fig. 15 L1 binned rms for raw carrier phase observable when a 10th order polynomial PCV is estimated in residual processing.

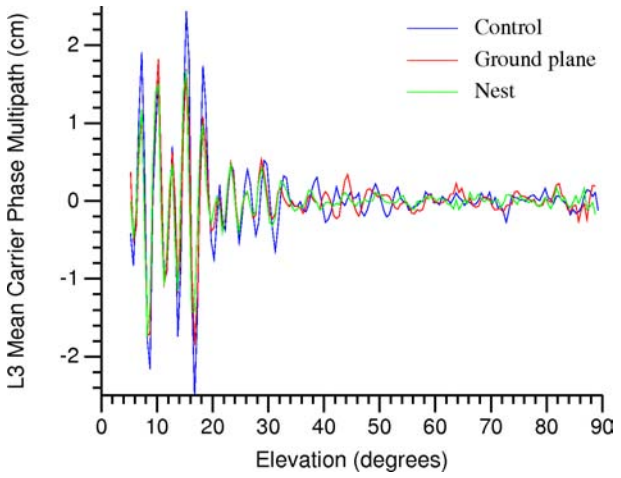

Fig. 16 L3 binned mean for raw carrier phase observable when a 10th order polynomial PCV is estimated in residual processing.

than for the code observable. This is an expected result since the SD carrier phase processing approach used here will tend to under-estimate the change in multipath reception due to modifying the antenna, as discussed previously.

Table 2 Total SD carrier phase rms error (in cm). Percentages indicate reduction relative to the control case.

	L1		L2		L3	
Case	RMS	%	RMS	%	RMS	%
Control	0.53	-	0.69	-	1.30	-
Gr. plane	0.51	3.8	0.61	11.6	1.13	13.1
Nest	0.48	9.4	0.59	14.5	1.08	16.9

Carrier Phase Smoothed Observables

As described previously, the carrier phase smoothed observables, and the NGA precise ephemeris were used to calculate ORDs. The ORDs were sorted by elevation and used to calculate binned statistics. A much larger bin size, 10 °, was used in this case than for the raw observables due to the much lower rate of the smoothed observables, 5 min. The binned rms of smoothed ORDs for the three AUT cases are compared in Fig. 18. It should first be noted that the multipath error in this observable is much lower, by a factor of 1.5 to 3, than in the L3 code multipath observable; this is the expected effect of the carrier smoothing process. On the other hand, significant multipath error, up to 0.7 m, still remains demonstrating that smoothing does not entirely remove multipath.

The behavior exhibited in the smoothed ORDs appears to be largely consistent with that of the raw observables, with the ground plane providing improvement over the control case for most angles, and the RF absorber nest providing further improvement. The degradation in performance due to the ground plane between $el = 50\,^\circ$ and $60\,^\circ$ as well as at $80\,^\circ$ appears to correspond to noted degradation at similar elevation angles in the L3 code multipath observable.

Table 3 Total rms error (in meters) in carrier phase smoothed ORDs. Percentages indicate reduction relative to the control case.

Case	RMS	%
Control	.39	
Gr. plane	.37	6.5
Nest	.27	30.5

Table 3 provides the total rms error calculated over all carrier phase smoothed ORDs for each AUT case. Despite the degradations noted at some angles in Fig. 18, the ground plane still offers an overall reduction, though modest, in the total rms multipath error in the smoothed observables. The performance improvement offered by the nest, however, is significant, $> 30\%$. These results suggest that both approaches would reduce multipath error contaminating GPS precise ephemeris products, but that an approach based upon the use of RF absorbing foam would be more effective.

CONCLUSIONS

Through the analysis of live sky measured GPS raw code and carrier phase observables as well as carrier-smoothed observables used in the generation of precise GPS ephemeris products, it has been demonstrated that it is possible to reduce multipath reception of a choke ring an-

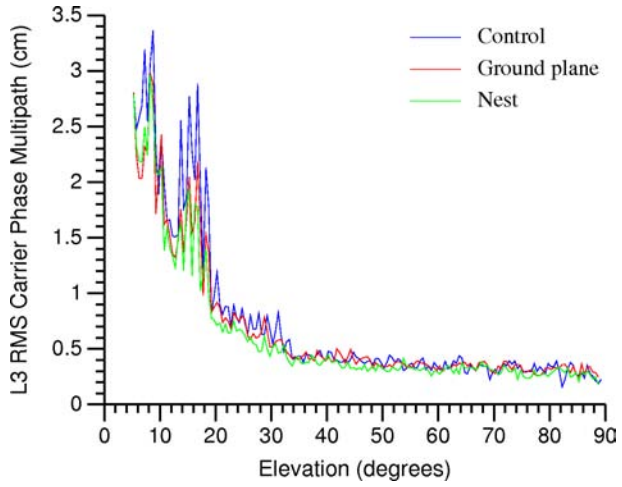

Fig. 17 L3 binned rms for raw carrier phase observable when a 10th order polynomial PCV is estimated in residual processing.

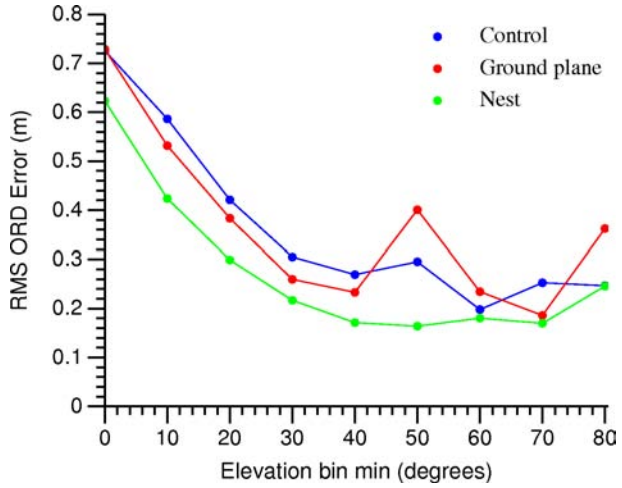

Fig. 18 The binned rms for observed range deviations (ORDs) for carrier phase smoothed observables.

tenna by placing a large metallic ground plane beneath or an appropriate arrangement of RF absorbing foam around the antenna. Further, it was shown that a novel RF absorbing foam nest design presented in this paper is significantly more effective at reducing multipath than a ground plane approach. These conclusions are consistent with the analysis of antenna radiation patterns generated using commercial electromagnetic simulation software, which was also presented in this paper.

These results might lead one at this point to simply adopt the RF absorbing foam nest design for use in reducing multipath reception at MSN stations. However, there are a number of other practical issues to consider as well. For instance, disadvantages of the RF absorbing foam nest approach are its higher design complexity and higher materials cost as compared with the relatively simple ground plane approach. It has yet to be determined how well the RF absorbing foam will hold up in the various climates in which MSN stations are located, although outdoor testing of the material in varied weather conditions in Austin, TX to date have been promising. For some stations, a potential issue with either approach is snow accumulation, which may change the electrical properties of the antenna or cause mechanical damage. Also, as was demonstrated in this paper, modifications to the choke ring antenna can alter its PCV pattern. Therefore, the modified choke ring antenna must be compatible, in terms of overall size and weight, with the method used to perform absolute PCV calibration, which is typically a live-sky robotic arm or motorized rotating platform approach. Finally, although it was demonstrated that these antenna modifications reduce multipath error in smoothed observables used in the generation of precise satellite ephemerides, it is critical to demonstrate that this improvement carries through to the final product itself. These issues will be the focus of continuing development, testing, and analysis.

ACKNOWLEDGMENTS

This effort was funded by the National Geospatial Intelligence Agency (NGA) through contract# N00024-07-D-6200, task# 5101045 and the ARL:UT Honor Scholar's program. The authors would like to acknowledge Robert F. Wong and Clifton F. Minter of NGA for their consultation regarding NGA ephemeris production, Jon Little of ARL:UT for establishing the ITT receiver data collection setup and making it available for this effort, and past ARL:UT students Kacie Walch and Scott Marmillion who contributed to the results presented in this paper. The EPS Toolkit (www.epstk.de) was used to generate many of the data visualizations in this paper.

REFERENCES

[1] B. Wiley, D. Craig, D. Manning, J. Novak, R. Taylor, and L. Weingarth. NGA's role in GPS. In *Proceedings of the 19th International Technical Meeting of the Satellite Division of the Institute of Navigation*, pages 2111 – 2119, Ft. Worth, TX, September 26-29 2006.

[2] Ron Hatch. The Synergism of GPS Code and Carrier Measurements. In *Proceedings of the 3rd International Symposium on Satellite Doppler Positioning*, Las Cruces, New Mexico, 1982.

[3] Robert B. Harris. *Incorporation of the Global Positioning System Modernization Signals into Existing Smoother-based Ephemeris Generation Processes*. PhD thesis, University of Texas at Austin, 2008.

[4] K.-D. Park, R.S. Nerem, M.S. Schenewerk, and J.L.Davis. Site-specific multipath characteristics of global IGS and CORS GPS sites. *Journal of Geodesy*, 77(12):799–803, June 2004.

[5] J. Ray. Systematic errors in GPS position estimates, presented at the IGS Workshop 2006, May 2006.

[6] M. DiBenedetto M. Braasch F. van Graas C. Bartone D.B. Thornberg, D.S. Thornberg. The LAAS integrated multipath limiting antenna (IMLA). In *Proceedings of the 15th International Technical Meeting of the Satellite Division of the Institute of Navigation*, Portland, Oregon, September 2002.

[7] J. Cicero. Personal communication regarding the U.S. Air Force GPS Monitor Station Antenna Replacement (MSAR) project, July 22, 2010.

[8] Constantine A. Balanis. *Advanced Engineering Electromagnetics*. John Wiley & Sons, New York, 1989.

[9] HFSS software. http://www.ansoft.com/products/hf/hfss/.

[10] Changdon Kee and Bradford Parkinson. Calibration of multipath errors on GPS pseudorange measurements. In *Proceedings of the 7th International Technical Meeting of the Satellite Division of the Institute of Navigation*, pages 353 – 362, Salt Lake City, UT, September 20-23 1994.

[11] R. Benjamin Harris. Evaluation, Refinement and Fusion of Software-Based Pseudorange Multipath Mitigation Techniques. In *Proceedings of the 15th International Technical Meeting of the Satellite Division of the Institute of Navigation*, Portland, Oregon, September 2002.

[12] G. Mader. GPS antenna calibration at the National Geodetic Survey. *GPS Solutions*, 3(1):50–58, 1999.

[13] Description of the Smoothing Algorithm in the NGA Monitor Station Network. Technical report, Applied Research Laboratories, The University of Texas at Austin, May 1998.

[14] GPSTk website. http://www.gpstk.org/.

[15] R. van Nee. Spread-spectrum code and carrier synchronization errors caused by multipath and interference. *IEEE Trans. Aerospace and Electronic Systems*, 29(4):1359–1365, 1993.